BioMACROMOLECULES

Article

pubs.acs.org/Biomac

# Specific Drug Formulation Additives: Revealing the Impact of Architecture and Block Length Ratio

Sebastian Wieczorek,[†] Timm Schwaar,[†,§] Mathias O. Senge,[‡] and Hans G. Börner*[,†]

[†]Department of Chemistry, Laboratory for Organic Synthesis of Functional Systems, Humboldt-Universität zu Berlin, Brook-Taylor-Str. 2, D-12489 Berlin, Germany

[‡]School of Chemistry, SFI Tetrapyrrole Laboratory, Trinity Biomedical Sciences Institute, Trinity College Dublin, The University of Dublin, 152-160 Pearse Street, Dublin, 2, Ireland

Supporting Information

**ABSTRACT:** Combining poly(ethylene glycol) (PEG) with sequence-defined peptides in PEG–peptide conjugates offers opportunities to realize next-generation drug formulation additives for overcoming undesired pharmacological profiles of difficult small molecule drugs. The tailored peptide segments provide sequence-specific, noncovalent drug binding, and the hydrophilic PEG block renders the complexes water soluble. On the basis of a peptide sequence known to bind the photosensitizer *m*-tetra(hydroxyphenyl)chlorin (*m*-THPC) for photodynamic cancer therapy, a set of different conjugate architectures is synthesized and studied. Variations in PEG block length and amplification of the peptidic binding domain of PEG–peptide conjugates are used to fine tune critical parameters for hosting *m*-THPC, such as drug payload capacities, aggregation sizes, and drug release and activation kinetics.

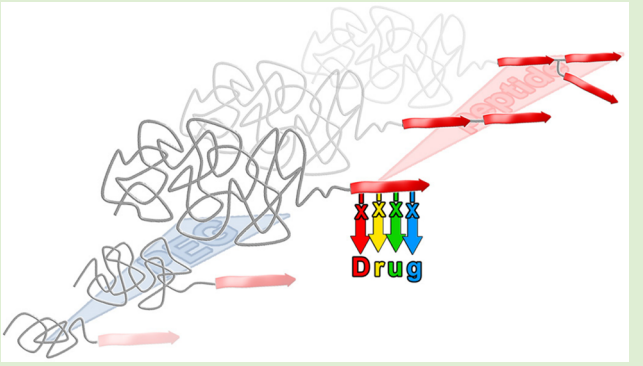


## INTRODUCTION

In recent decades, defined macromolecules and amphiphilic block copolymers have proved to be highly valuable as drug formulation additives, improving the performance of difficult drugs as well as enabling the realization of novel concepts for drug delivery and targeting.[1−8] One focus of modern pharmacological drug design has been progressively set on hydrophobic small molecule drugs, resulting in a demand for polymeric coadditives, which provide solubility, mediate bioavailability, and prevent undesired partitioning of the compounds.[9−11] Despite a few very promising novel platforms,[12−16] the set of investigated polymers and resulting block copolymers is largely limited to FDA approved polymers that restrict the chemical variability for block copolymer formulation additives.[17,18] Bioconjugates that combine poly(ethylene glycol) (PEG) and sequence-defined peptides comprise a polymer family denoted precision polymers, which are highly information rich, cover an enormous chemical space, and have sharply definable sequence–property relationships.[19−22] This class of peptide–polymer conjugates proved to have broad applicability, ranging from tailored drug solubilizers to self-assembled nano- and microstructures for cell growth scaffolds to enzymatically activable coatings or glues to anisotropic soft matter structures for molecular electronics or directed composite formation.[23−36] Precision polymers exhibit rich opportunities in the field of biomedicine, enabling insights to be revealed into the behavior of multifunctional macromolecules in complex biological environments. Recently, Wagner et al. utilized precision polymers to progress the fundamental understanding of aspects of the process that occurs in dsDNA or siRNA delivery.[37] Hartmann et al. elucidated lectin binding modes of multivalent substrates to identify molecular parameters relevant for ligand binding or substrate clustering.[38] Börner et al. showed that peptide–PEG conjugates could be tailored by either empirically or combinatorially assisted design to enable sequence-specific hosting of problematic drug molecules.[39−41] Those specific solubilizers rendered kinase IpsE inhibitors or *m*-tetra(hydroxyphenyl)chlorin (*m*-THPC)[42] photosensitizers with undesired pharmacological profiles readily available for biotesting or biodistribution. The platform of specific solubilizers offers opportunities to cost effectively overcome solubility issues of polar water insoluble small organic lead compounds or drug entities without tedious, cost intensive drug structure adaption cycles. However, structure–property relationships to optimize specific drug solubilizers, improving payload and tailoring drug/solubilizer complexation strength, are not yet well understood.

Here, we provide insights into structure–property relationships of peptide–PEG conjugates for the solubilization of an *m*-

Received: July 17, 2015
Revised: August 24, 2015





DOI: 10.1021/acs.biomac.5b00961
Biomacromolecules XXXX, XXX, XXX−XXX

THPC photosensitizer. The study reveals the dependencies of drug loading capacity and drug activation kinetics on the architecture of the utilized peptide–PEG conjugates by systematically altering the (1) peptide segment length, (2) segment architecture, and (3) PEG–peptide block length ratio.

## EXPERIMENTAL SECTION

A detailed description of materials, instrumentation, experimental procedures, and analytical data is available as Supporting Information.

Peptide–PEG conjugates (**P-PEG$_{0.85k}$**, **P-PEG$_{3.2k}$**, **P-PEG$_{5.2k}$**, **P2-PEG$_{5.2k}$**, and **P3-PEG$_{5.2k}$**) were obtained by automated solid-phase peptide synthesis on an ABI 433a peptide synthesizer (Applied Biosystems) using Tentagel-PAP resins as solid support preloaded with PEG (approximately 0.85, 3.2, and 5.2 kg/mol). After stepwise polypeptide assembly via a HBTU/NMP/piperidine protocol, conjugates were cleaved from the solid support by treatment with a mixture of 95% TFA, 4% TES, and 1% $H_2O$, precipitated in cold diethyl ether, and dialyzed against deionized water (100–500 or 500–1000 Da MWCO, cellulose ester). Peptide conjugates were characterized by MALDI-ToF-MS, $^1$H nuclear magnetic resonance spectra ($^1$H NMR) in TFA-$d_1$, and Fourier transform infrared spectroscopy (ATR-FT-IR).

For solubilization of *m*-THPC by peptide–PEG conjugates, *m*-THPC was dissolved in EtOH (1 mg/mL) and 1 mL (1.47 $\mu$mol of *m*-THPC) of the solution was added to solutions of each carrier (1.47 $\mu$mol) in deionized water (1 mL, pH 7). The resulting mixtures were shaken for 1 h and freeze-dried *in vacuo*. Residues were dissolved in deionized water (1 mL, pH 7), followed by centrifugation to remove any *m*-THPC that was not solubilized. Supernatants were diluted with EtOH to avoid aggregation, and the concentration of solubilized *m*-THPC was determined by UV–vis spectroscopy.

Drug trans-solubilzation to BSA was studied by fluorescence emission spectroscopy. Time-resolved fluorescence emission was recorded on a microplate reader in black polystyrene 96-well plates. None of the tested carrier systems showed distinct fluorescence emission upon saturation with their individual maximum payload of *m*-THPC (Supporting Information). To trigger fluorescence emission, a solution of BSA in deionized water was added to samples of *m*-THPC-loaded carriers. Immediately, fluorescence emission ($\lambda_{em}$, 654 nm; $\lambda_{exc}$, 417 nm) was recorded with a 2 min delay for a period of 18 h and plotted against time.

## RESULTS AND DISCUSSION

Previously, a combinatorial strategy revealed a peptide–PEG conjugate that effectively solubilized the partially approved *m*-THPC photosensitizer, which is used for photodynamic cancer therapy.[40] From a single bead/single component library of about $8.2 \times 10^5$ different peptides, the sequence Gln-Phe-Phe-Leu-Phe-Phe-Gln (QFFLFFQ) was selected and studied, demonstrating solubilization of *m*-THPC with a payload of 1:3.3 (drug/solubilizer). Drug transport occurs in a silent (nonactive) drug state. However, trans-solubilization, e.g., to blood-plasma protein models like albumins, generates the active form of the drug that exhibits singlet oxygen production upon irradiation with 652 nm light.

To study the influence of the PEG polymer block length and the peptide binding segment on *m*-THPC solubilization and drug release kinetics, two different sets of peptide–PEG conjugates were synthesized and analyzed (Figure 1). On one hand, the nonfunctional PEG segment, responsible for water solubility and drug shielding, was altered ($M_n$ = 850, 3200, and 5200 g/mol) while the peptide segment was kept unchanged (QFFLFFQ-*block*-PEG$_x$, Figure 1, **P-PEG$_{0.85k}$**, **P-PEG$_{3.2k}$**, and **P-PEG$_{5.2k}$**). On the other hand, the PEG block length was kept constant ($M_n$ = 5200 g/mol) and the peptide segments, responsible for specific noncovalent drug binding, were

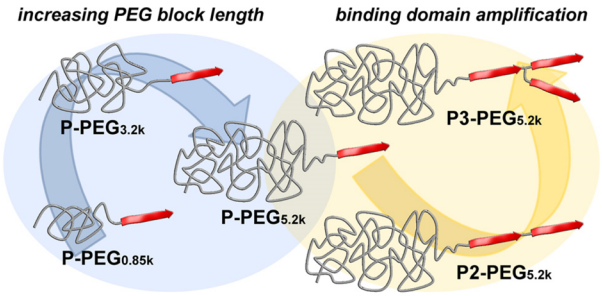


**Figure 1.** Schematic illustration of the systematic variation of peptide–PEG conjugate architectures: altering the PEG block length (**P-PEG$_{0.85k}$**, **P-PEG$_{3.2k}$**, and **P-PEG$_{5.2k}$**) and the peptidic binding segment (**P-PEG$_{5.2k}$**, **P2-PEG$_{5.2k}$**, **P3-PEG$_{5.2k}$**).

changed from linear monovalent to linear bivalent to branched trivalent (Figure 1, **P-PEG$_{5.2k}$**, **P2-PEG$_{5.2k}$**, **P3-PEG$_{5.2k}$**). The conjugates were synthesized via an inverse conjugation approach by solid-phase-supported peptide synthesis (SPPS) using supports preloaded with the proper PEG blocks.[43] The inverse conjugation strategy enables the different peptide segments to be sequentially synthesized at the supported PEG blocks and the fully deprotected peptide–PEG conjugates to be liberated from the synthesis resins. The linear constructs **P-PEG$_{0.85k}$**, **P-PEG$_{3.2k}$**, **P-PEG$_{5.2k}$**, and **P2-PEG$_{5.2k}$** were obtained in a straightforward manner. In the case of the bis-valent **P2-PEG$_{5.2k}$**, the second peptide binding domain was linked via a flexible 6-amino hexanoic acid moiety (Fmoc-Ahx-OH). To introduce a branching point between the three peptide domains of the tris-valent **P3-PEG$_{5.2k}$**, a $\alpha,\varepsilon$-Fmoc-diprotected lysine derivative (Fmoc Lys(Fmoc)-OH) was coupled after completing the linking of the first peptide binding domain. In the ongoing SPPS, two peptide chains grow parallel with the same sequence from both the $\alpha$- and $\varepsilon$-amino groups of the lysine residue, resulting in a Y-shaped motif. After liberation from the supports, the different peptide–PEG conjugates were isolated in a fully deprotected manner, and their chemical identities were proven by mass spectrometry (MALDI-ToF-MS) and $^1$H NMR (Supporting Information).

To study the effect of PEG length and peptide architecture on maximum cargo capacity and payload, the set of peptide conjugates was loaded with *m*-THPC using an established freeze-drying methodology to force loading.[40] For that purpose, *m*-THPC was dissolved in ethanol and mixed with the aqueous solutions of the corresponding bioconjugates. After freeze drying of the mixtures and resuspension in water, the excess *m*-THPC could be removed by centrifugation, and drug concentration in the supernatant was determined by UV–vis spectroscopy (Figure 2).

As is evident, alterations within the peptide part of the bioconjugates seem to have more pronounced effects on *m*-THPC's solubilization capacity compared to that due to changes in the length of the PEG block (Table 1). Systematically increasing the number of peptide binding domains per bioconjugate molecule, from linear monobinder to linear bis-binder to star-shaped tris-binder, resulted in a significant impact on drug solubilization efficiency. Comparing **P-PEG$_{5.2k}$** with **P2-PEG$_{5.2k}$** demonstrates that doubling the peptide segment in a linear fashion increases the molar drug payload from 1:3.4 to 1:1.4 (drug/carrier). Although **P2-PEG$_{5.2k}$** solubilizes 0.74 mmol of *m*-THPC per mmol conjugate, **P3-PEG$_{5.2k}$** reached a capacity of 0.95 mmol per


DOI: 10.1021/acs.biomac.5b00961
Biomacromolecules XXXX, XXX, XXX–XXX

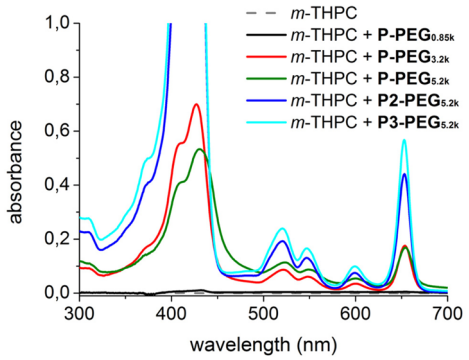


**Figure 2.** UV−vis absorption spectra of *m*-THPC/carrier complexes in water indicating successful drug solubilization by peptide−PEG conjugates compared to that of the free drug without formulation additives (conditions: *c*[conjugates] = 15 $\mu$M in water, rt, pH 7).

**Table 1. Hydrodynamic Radii of Conjugate Carrier Aggregates in Water Prior to and after Loading with Maximum Amounts of *m*-THPC Determined by Dynamic Light Scattering and Maximum Drug Payload Capacity of Conjugate Carriers Determined by UV−vis Absorbance Spectroscopy**[a]

| | $R_h$ [nm] | | | |
|---|---|---|---|---|
| carrier | −*m*-THPC | +*m*-THPC | payload (drug/carrier) in [mmol/mmol] | molar drug-to-carrier ratio |
| **P-PEG$_{3.2k}$** | 37 ± 5 | 165 ± 22 | 0.31 | 1:3.3 |
| **P-PEG$_{5.2k}$** | 13 ± 5 | 120 ± 4 | 0.30 | 1:3.4 |
| **P2-PEG$_{5.2k}$** | 35 ± 3 | 110 ± 18 | 0.74 | 1:1.4 |
| **P3-PEG$_{5.2k}$** | 25 ± 2 | 65 ± 7 | 0.95 | 1:1.1 |

[a]Conditions: DLS: *c*[conjugates] = 0.37 mM in water, rt, pH 7; UV−vis: *c*[conjugates] = 15 $\mu$M in water/EtOH 1:99, rt.

mmol of conjugate (1:1.1 molar drug/carrier). Thus, it was possible to gain a 2- and 3-fold higher payload capacity by doubling and tripling the binding amino acid sequence, respectively. It is most likely that the further increase in the payload capacity of **P3-PEG$_{5.2k}$** compared to that of **P2-PEG$_{5.2k}$** is not exclusively a consequence of having more copies of the binding domain but also could result partially from the branched architecture of **P3-PEG$_{5.2k}$** compared to the linear **P2-PEG$_{5.2k}$** conjugate. Increasing the length of the solubility-providing PEG block apparently does not influence the maximum cargo dramatically. **P-PEG$_{3.2k}$** and **P-PEG$_{5.2k}$**, with PEG block lengths of 3200 and 5200 g/mol, showed drug loading ratios of 0.31 and 0.30 mmol of *m*-THPC per mmol of conjugate, respectively. Whereas **P-PEG$_{3.2k}$** reaches a molar payload of 1:3.3 (drug/carrier), **P-PEG$_{5.2k}$** yields an almost identical payload of 1:3.4. Interestingly, having a critical PEG length seems to be necessary, as **P-PEG$_{0.85k}$** brought practically no *m*-THPC into solution. That there is a lower limit of the PEG length is not surprising considering that the peptide segment has a molecular weight of 976 Da and is rather hydrophobic.

To understand the impact of amino acid sequence, architectural parameters, and *m*-THPC loading on solubilization, the different peptide−PEG conjugates were investigated prior to and after drug loading (Table 1). Dynamic light scattering (DLS) on dilute aqueous solutions of bioconjugates confirmed the amphiphilic character of the PEG−peptide conjugates. All samples indicate the formation of block copolymer aggregates in the absence of *m*-THPC within a hydrodynamic radii window of $R_h$ = 13−37 nm (Table 1). Consistent with the aggregation theory of amphiphilic block copolymers, increasing the hydrophilic PEG block with the peptide segments held constant leads to smaller aggregates (cf. **P-PEG$_{3.2k}$** and **P-PEG$_{5.2k}$**).[44] Moreover, when keeping the PEG block length unchanged, aggregate sizes become larger as the rather hydrophobic peptide segment increases due to the shift in hydrophobicity from **P-PEG$_{5.2k}$** to **P2-PEG$_{5.2k}$**. **P3-PEG$_{5.2k}$** shows a reduced hydrodynamic radius compared to that of **P2-PEG$_{5.2k}$**, which could potentially indicate a more dense packing of the hydrophobic peptides due to the compact branched topology or a change in the type of aggregate formed. As expected, the hydrodynamic radii of all solubilizer aggregates increased during loading with hydrophobic *m*-THPC (Table 1). The increase in the aggregate size of the loaded bioconjugates is less significant in response to increasing the molecular weight of the carriers. Whereas the smallest bioconjugate, **P-PEG$_{3.2k}$**, showed the highest increase from $R_h$ = 37 to 165 nm, loading of the largest solubilizer, **P3-PEG$_{5.2k}$**, led to the lowest increase of $R_h$, from 25 to 65 nm. These results can be understood by taking into account that, in all cases, there was a rather constant ratio of peptidic 7-mer binding domains per *m*-THPC. One drug molecule required, on average, roughly three peptide binding domains to be effectively solubilized. Because **P3-PEG$_{5.2k}$** provides (with three peptide binding domains per carrier molecule) this ideal ratio, only minor changes in aggregation seem to be required. In contrast, **P-PEG$_{3.2k}$** (exhibiting a small hydrophilic PEG block and a single peptide binding domain) has to reorganize to a large extent to saturate the *m*-THPC molecules' surface with an appropriate number of peptide domains and to provide sufficient PEG for colloidal stability.

Regardless of the solubilizer and the differences in drug loading and aggregation size, all *m*-THPC-loaded systems show strongly reduced or no fluorescence emission (Supporting Information). This indirectly indicates the high packing density and intermolecular quenching of the *m*-THPC fluorophores in the aggregates. Such a silent transport mode appears to be advantageous for photodynamic therapy, as beneficial effects on shelf-life time and reduced risk during handling of the drug formulation would be anticipated. However, due to high binding affinity of *m*-THPC to blood plasma proteins,[45,46] trans-solubilization of the sensitizer to, e.g., serum albumin takes place (Figure 3). This results in subsequent monomerization of aggregated *m*-THPC, reducing quenching as the drug develops into an active form.[40,47] The impact of different conjugate architectures on sensitizer trans-solubilization to bovine serum albumin (BSA) as a model protein was examined by following drug activation kinetics via fluorescence emission spectroscopy. As **P-PEG$_{0.85k}$** failed to solubilize *m*-THPC, only conjugates with PEG block lengths of 3200 and 5200 g/mol were compared (Figure 3). A large excess of BSA was given to aqueous solutions of conjugate carriers loaded with their respective maximum payload of *m*-THPC. Time-resolved fluorescence measurements show, for all solubilization systems, an increase in the fluorescence intensity, which was previously demonstrated to coincide with singlet oxygen production capability.[40] Strong differences in the drug activation kinetics could be found, depending on the formulation additives used. Fluorescence emission of *m*-THPC solubilized by **P-PEG$_{3.2k}$** compared to that by **P-PEG$_{5.2k}$** increased considerably slower. For instance, *m*-THPC/**P-PEG$_{3.2k}$** complexes exhibited only


DOI: 10.1021/acs.biomac.5b00961
Biomacromolecules XXXX, XXX, XXX−XXX

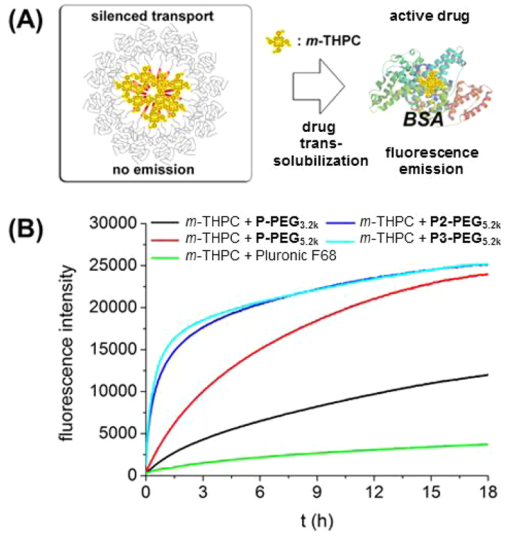


**Figure 3.** Schematic illustration of trans-solubilization from *m*-THPC/solubilizer complexes to BSA (PDB 3V03) as a blood serum protein model, resulting in drug transfer and drug activation (A). Corresponding *m*-THPC activation kinetics followed by time-resolved fluorescence emission to compare the effects of PEG block length and peptide segment architecture with a control experiment using Pluronic F68 as a commonly established formulation additive (B) (conditions: $\lambda_{ex}$, 417 nm; $\lambda_{em}$, 654 nm; $c$[BSA] = 100 $\mu$M; $c$[*m*-THPC] = 0.1 $\mu$M).

~50% of the fluorescence intensity that was reached by *m*-THPC/**P-PEG$_{5.2k}$** complexes after an 18 h incubation with BSA. This is counterintuitive, as a higher PEG block length was expected to show advanced drug shielding and to retard sensitizer trans-solubilization to BSA. Considering the smaller aggregate sizes found for drug-loaded **P-PEG$_{5.2k}$** compared to that for loaded **P-PEG$_{3.2k}$**, a larger interface area is provided by the *m*-THPC/**P-PEG$_{5.2k}$** complexes. This could potentially result in an increase in the effective collision events between proteins and drug/complexes required to promote drug trans-solubilization from aggregates to BSA. A diffusion mechanism via unimer exchange and transport is less likely because solubilizers **P2-PEG$_{5.2k}$** and **P3-PEG$_{5.2k}$**, with larger hydrophobic segments, show even higher drug−BSA transfer rates.

The di- and trimerization of the peptide binding domains in a linear or branched manner gave rise to solubilizers that combine having a high payload capacity with remarkable rates for drug activation (Figure 3, **P-PEG$_{5.2k}$**, **P2-PEG$_{5.2k}$**, and **P3-PEG$_{5.2k}$**). The increase in fluorescence after BSA addition was obviously faster compared to activation from *m*-THPC/**P-PEG$_{3.2k}$** complexes. Fluorescence intensities reach, in all cases, roughly similar values after 18 h. Nevertheless, the slopes of *m*-THPC activation kinetics varied dramatically depending on the utilized solubilizers. Within 2 h, ~65 and ~70% of the entire drug load was found to have been already activated from *m*-THPC/**P2-PEG$_{5.2k}$** or *m*-THPC/**P3-PEG$_{5.2k}$** complexes, respectively. By then, only 30% of the drug was activated from *m*-THPC/**P-PEG$_{5.2k}$** complexes. Rapid drug activation is clearly desired for photodynamic therapy applications because irradiation treatment might start 2 h after administration of the sensitizers and because retarding the release of the active drug into the biosystem afterward should be minimized. The impressive differences and opportunities arising from tailored specific drug formulation additives can be seen by using Pluronic F68 as a common triblock copolymer[48] additive to solubilize *m*-THPC. Fluorescence kinetics indicate that the drug activation rate was significantly slower with *m*-THPC/F68 complexes as compared to that with drug complexes of all conjugate solubilizers, showing that the criteria of rapid drug activation cannot be met. Within 18 h, only 15% of the drug was activated with respect to the amounts found to be activated with *m*-THPC/**P2-PEG$_{5.2k}$** or *m*-THPC/**P3-PEG$_{5.2k}$** complexes. It should be emphasized that accurately adjusting the interaction capabilities between a drug and carrier results not only in an optimized drug loading capacity but also in drug release profiles that are adapted for a specific purpose, which is not easily and accurately adjustable with commonly used block copolymer-based formulation additives.

The general trend of accelerated drug release following an increase in the payload capacity of the conjugate carriers and a decrease in aggregate sizes is consistent. This can be explained by the decreasing excess of conjugate necessary for effective drug solubilization and colloidal stability. Simultaneously, the hydrodynamic radii of drug/conjugate aggregates are diminishing. It can be assumed that a lower drug-to-carrier ratio due to a higher payload capacity might reduce the PEG shell's shielding effect against proteins. This could potentially cause a significant promotion of drug transfer to BSA molecules, as observed for **P2-PEG$_{5.2k}$** and **P3-PEG$_{5.2k}$** compared to **P-PEG$_{5.2k}$**.

## CONCLUSIONS

Tailor-made formulation additives have been studied to render *m*-THPC as a partially approved water-soluble photosensitizer and to potentially overcome undesired pharmacological profiles by improving bioavailability for photodynamic cancer therapy. A set of specific solubilizers was designed and synthesized based on peptide−PEG conjugates that comprise a combinatorially selected peptide segment as a binding domain to host *m*-THPC. The solubilizers vary systematically in PEG block length ($M_{n,PEG}$ = 850, 3200, and 5200 g/mol) and in the architecture of the peptidic drug binding domain (monomeric 7-mer domain, linear dimeric domain, and branched trimeric domain). The drug formulation additives were investigated with respect to maximum payload capacities, aggregate sizes, and drug release/activation profiles. Conceptionally, the peptide segment determines drug binding and hosting. Thus, increasing the PEG block length from 3200 to 5200 g/mol did not have a significant effect on the *m*-THPC payload capacity. However, an adequate PEG block length seems to be required to provide sufficient water solubility and colloidal stability to the drug/solubilizer complexes, as **P-PEG$_{8.5k}$** was not able to solubilize *m*-THPC. The drug payload capacity of conjugates could be doubled and tripled by amplification of the peptide segments from a linear monobinding domain to a linear bis-valent and branched trivalent domain, respectively. All solubilizers transport *m*-THPC in a nonactive (silent) transport form. However, drug activation occurs by trans-solubilization of *m*-THPC from drug/solubilizer complexes to albumins as a model of blood plasma protein. Drug activation kinetics could be precisely adjusted over a broad range according to the needs of the therapeutic approach. The activation kinetics show a pronounced dependence on the aggregate sizes of the *m*-THPC/conjugate complexes. It is most likely that, due to kinetic control during the forced drug loading procedure, a reduction in aggregate sizes could be achieved by increasing either the PEG block length or the valency of the peptidic binding domain. A general trend was found in which more rapid trans-solubilization and drug activation occurred from


DOI: 10.1021/acs.biomac.5b00961
Biomacromolecules XXXX, XXX, XXX−XXX

drug/solubilizer complexes as the drug payload increased and aggregate sizes decreased. This most likely reflects the relevance of the interfacial area, providing effective contacts between albumin proteins and drug/conjugate aggregates. This study underlines the opportunities for precisely adjusting peptide−PEG conjugates for solubilization of water insoluble, polar small drug molecules. It should be emphasized that combining a combinatorial approach to select peptide sequences that specifically bind small organic molecules in a noncovalent manner with different conjugate architectures can enrich the toolbox and lead to the next generation of precisely definable drug formulation additives.

## ■ ASSOCIATED CONTENT

### Supporting Information

The Supporting Information is available free of charge on the ACS Publications website at DOI: 10.1021/acs.biomac.5b00961.

Materials, instrumentation, experimental procedures, and analytical data (PDF).

## ■ AUTHOR INFORMATION


### Corresponding Author

*E-mail: h.boerner@hu-berlin.de; Phone: +49 (0)30-2093 7348; Fax: +49 (0)30 2093-7266.

### Present Address

§(T.S.) German Federal Institute for Materials Research and Testing (BAM), Richard-Willstätter-Str. 11, D-12489 Berlin, Germany.


### Notes

The authors declare no competing financial interest.

## ■ ACKNOWLEDGMENTS

The authors acknowledge Antje Völkel, Helmut Schlaad (The Max Planck Institute of Colloids and Interfaces, Potsdam-Golm), and Felix Hanßke (HU Berlin) for DLS measurements. Funding was granted from the European Research Council under the European Union's 7th Framework Program (FP07-13)/ERC Starting grant "Specifically Interacting Polymers−SIP" (ERC 305064).

## ■ REFERENCES


(1) Peer, D.; Karp, J. M.; Hong, S.; FaroKhzad, O. C.; Margalit, R.; Langer, R. *Nat. Nanotechnol.* **2007**, *2*, 751.
(2) Duncan, R. *Nat. Rev. Drug Discovery* **2003**, *2*, 347.
(3) Allen, T. M.; Cullis, P. R. *Science* **2004**, *303*, 1818.
(4) Checot, F.; Lecommandoux, S.; Gnanou, Y.; Klok, H. A. *Angew. Chem., Int. Ed.* **2002**, *41*, 1339.
(5) Kataoka, K.; Harada, A.; Nagasaki, Y. *Adv. Drug Delivery Rev.* **2001**, *47*, 113.
(6) Liechty, W. B.; Kryscio, D. R.; Slaughter, B. V.; Peppas, N. A. *Annu. Rev. Chem. Biomol. Eng.* **2010**, *1*, 149.
(7) Kannan, R. M.; Nance, E.; Kannan, S.; Tomalia, D. A. *J. Intern. Med.* **2014**, *276*, 579.
(8) Zhang, S. Y.; Zou, J.; Zhang, F. W.; Elsabahy, M.; Felder, S. E.; Zhu, J. H.; Pochan, D. J.; Wooley, K. L. *J. Am. Chem. Soc.* **2012**, *134*, 18467.
(9) Paul, S. M.; Mytelka, D. S.; Dunwiddie, C. T.; Persinger, C. C.; Munos, B. H.; Lindborg, S. R.; Schacht, A. L. *Nat. Rev. Drug Discovery* **2010**, *9*, 203.
(10) Di, L.; Fish, P. V.; Mano, T. *Drug Discovery Today* **2012**, *17*, 486.
(11) Williams, H. D.; Trevaskis, N. L.; Charman, S. A.; Shanker, R. M.; Charman, W. N.; Pouton, C. W.; Porter, C. J. H. *Pharmacol. Rev.* **2013**, *65*, 315.
(12) Sun, J.; Zuckermann, R. N. *ACS Nano* **2013**, *7*, 4715.
(13) Huesmann, D.; Sevenich, A.; Weber, B.; Barz, M. *Polymer* **2015**, *67*, 240.
(14) Steinbach, T.; Wurm, F. R. *Angew. Chem., Int. Ed.* **2015**, *54*, 6098.
(15) Luxenhofer, R.; Han, Y.; Schulz, A.; Tong, J.; He, Z.; Kabanov, A. V.; Jordan, R. *Macromol. Rapid Commun.* **2012**, *33*, 1613.
(16) Huang, J.; Bonduelle, C.; Thevenot, J.; Lecommandoux, S.; Heise, A. *J. Am. Chem. Soc.* **2012**, *134*, 119.
(17) Mansour, H. M.; Sohn, M.; Al-Ghananeem, A.; DeLuca, P. P. *Int. J. Mol. Sci.* **2010**, *11*, 3298.
(18) Knop, K.; Hoogenboom, R.; Fischer, D.; Schubert, U. S. *Angew. Chem., Int. Ed.* **2010**, *49*, 6288.
(19) Börner, H. G. *Macromol. Rapid Commun.* **2011**, *32*, 115.
(20) Lutz, J.-F.; Ouchi, M.; Liu, D. R.; Sawamoto, M. *Science* **2013**, *341*, 1238149.
(21) Lutz, J.-F. *Acc. Chem. Res.* **2013**, *46*, 2696.
(22) Lutz, J.-F. *Macromolecules* **2015**, *48*, 4759.
(23) Deacon, S. P. E.; Apostolovic, B.; Carbajo, R. J.; Schott, A.-K.; Beck, K.; Vicent, M. J.; Pineda-Lucena, A.; Klok, H.-A.; Duncan, R. *Biomacromolecules* **2011**, *12*, 19.
(24) Georgieva, J. V.; Brinkhuis, R. P.; Stojanov, K.; Weijers, C.; Zuilhof, H.; Rutjes, F.; Hoekstra, D.; van Hest, J. C. M.; Zuhorn, I. S. *Angew. Chem., Int. Ed.* **2012**, *51*, 8339.
(25) Danial, M.; Root, M. J.; Klok, H.-A. *Biomacromolecules* **2012**, *13*, 1438.
(26) Hartmann, L.; Börner, H. G. *Adv. Mater.* **2009**, *21*, 3425.
(27) Börner, H. G. *Prog. Polym. Sci.* **2009**, *34*, 811.
(28) Gentsch, R.; Boysen, B.; Lankenau, A.; Börner, H. G. *Macromol. Rapid Commun.* **2010**, *31*, 59.
(29) Kühnle, R. I.; Börner, H. G. *Angew. Chem., Int. Ed.* **2011**, *50*, 4499.
(30) Bode, S. A.; Hansen, M. B.; Oerlemans, R.; van Hest, J. C. M.; Lowik, D. *Bioconjugate Chem.* **2015**, *26*, 850.
(31) Wilke, P.; Helfricht, N.; Mark, A.; Papastavrou, G.; Faivre, D.; Börner, H. G. *J. Am. Chem. Soc.* **2014**, *136*, 12667.
(32) Schwemmer, T.; Baumgartner, J.; Faivre, D.; Börner, H. G. *J. Am. Chem. Soc.* **2012**, *134*, 2385.
(33) Jahnke, E.; Lieberwirth, I.; Severin, N.; Rabe, J. P.; Frauenrath, H. *Angew. Chem., Int. Ed.* **2006**, *45*, 5383.
(34) Shaytan, A.; Schillinger, E.-K.; Khalatur, P.; Mena-Osteritz, E.; Hentschel, J.; Börner, H. G.; Bäuerle, P.; Khokhlov, A. *ACS Nano* **2011**, *5*, 6894.
(35) Díez, I.; Hahn, H.; Ikkala, O.; Börner, H. G.; Ras, R. H. A. *Soft Matter* **2010**, *6*, 3160.
(36) Hanßke, F.; Kemnitz, E.; Börner, G. H. *Small* **2015**, DOI: 10.1002/smll.201500162.
(37) Wagner, E. *Acc. Chem. Res.* **2012**, *45*, 1005.
(38) Ponader, D.; Maffre, P.; Aretz, J.; Pussak, D.; Ninnemann, N. M.; Schmidt, S.; Seeberger, P. H.; Rademacher, C.; Nienhaus, G. U.; Hartmann, L. *J. Am. Chem. Soc.* **2014**, *136*, 2008.
(39) Hirsch, A. K. H.; Diederich, F.; Antonietti, M.; Borner, H. G. *Soft Matter* **2010**, *6*, 88.
(40) Wieczorek, S.; Krause, E.; Hackbarth, S.; Röder, B.; Hirsch, A. K. H.; Börner, H. G. *J. Am. Chem. Soc.* **2013**, *135*, 1711.
(41) Wieczorek, S.; Vigne, S.; Masini, T.; Ponader, D.; Hartmann, L.; Hirsch, A. K. H.; Börner, H. G. *Macromol. Biosci.* **2015**, *15*, 82.
(42) Senge, M. O. *Photodiagn. Photodyn. Ther.* **2012**, *9*, 170.
(43) Lutz, J.-F.; Börner, H. G. *Prog. Polym. Sci.* **2008**, *33*, 1.
(44) Antonietti, M.; Forster, S.; Oestreich, S. *Macromol. Symp.* **1997**, *121*, 75.
(45) Michael-Titus, A. T.; Whelpton, R.; Yaqub, Z. *Br. J. Clin. Pharmacol.* **1995**, *40*, 594.
(46) Reshetov, V.; Zorin, V.; Siupa, A.; D'Hallewin, M.-A.; Guillemin, F.; Bezdetnaya, L. *Photochem. Photobiol.* **2012**, *88*, 1256.




DOI: 10.1021/acs.biomac.5b00961
*Biomacromolecules* XXXX, XXX, XXX−XXX

(47) Reshetov, V.; Kachatkou, D.; Shmigol, T.; Zorin, V.; D'Hallewin, M.-A.; Guillemin, F.; Bezdetnaya, L. *Photochem. Photobiol. Sci.* **2011**, *10*, 911.
(48) Kabanov, A. V.; Alakhov, V. Y. *Crit. Rev. Ther. Drug Carrier Syst.* **2002**, *19*, 1.



DOI: 10.1021/acs.biomac.5b00961
*Biomacromolecules* XXXX, XXX, XXX−XXX